



ELSEVIER

Contents lists available at SciVerse ScienceDirect

International Journal of Plasticity

journal homepage: www.elsevier.com/locate/ijplas

Necking limit of substrate-supported metal layers under biaxial in-plane loading

Zheng Jia, Teng Li*

Department of Mechanical Engineering, University of Maryland, College Park, MD 20742, United States

ARTICLE INFO

Article history:

Received 26 February 2013

Received in final revised form 18 June 2013

Available online xxxx

Keywords:

Necking

Plasticity

Bilayer

Biaxial loading

Instability

ABSTRACT

Necking instability often indicates the onset of ductile failure. It has been shown that the necking instability in a substrate-supported metal layer can be retarded to a higher strain than that in a single freestanding metal layer. Most existing theoretical studies of the necking limit of substrate-supported metal layers assume plane strain condition. However, most commonly conducted experiments of such metal/substrate bilayers are uniaxial tensile tests. So far, the necking instability of substrate-supported metal layers under arbitrary combinations of biaxial in-plane loading conditions remains poorly understood. This paper presents a comprehensive study of the necking limit of a metal/substrate bilayer over the full range of biaxial loading ratio, from 1 for equibiaxial loading, to 0 for plane strain loading, and to $-1/2$ for uniaxial loading. Two representative material combinations are considered, namely, a metal layer supported by a stiff plastic substrate, and a metal layer supported by a compliant elastomer substrate. The results quantitatively correlate both critical necking limit strain and necking band orientation with the material properties and thickness ratio of the substrate-metal bilayer. In particular, the predicted necking band orientation when the bilayer is under in-plane loading with a negative ratio (e.g., uniaxial tension) agrees with the slanted necking bands observed in experiments, a phenomenon that cannot be explained by existing theoretical studies assuming plane strain condition. The present study further shows that necking retardation in an elastomer-supported metal layer can allow the bilayer to absorb and dissipate more energy than an all-metal single layer with the same mass. These understandings shed light on optimal design of substrate-supported metal structures with enhanced deformability and energy absorbing capacity under complex in-plane loading conditions.

© 2013 Elsevier Ltd. All rights reserved.

1. Introduction

Substrate-supported metal layers are being developed as structural elements and functional components in modern technologies, with the promise of enhanced mechanical performance in comparison with freestanding metal layers. For example, thin metal films deposited on polymer substrates are often used as deformable conductors and interconnects in flexible electronic devices that are often subject to large stretches, bends and twists (Cordill et al., 2010; Cotton et al., 2009; Graudejus et al., 2012; Lacour et al., 2006; Lacour et al., 2005; Li et al., 2004; Li et al., 2005b; Lu et al., 2010; Lu et al., 2007; Wagner et al., 2004; Xu et al., 2010). Polymer-coated metal layers have been shown to be able to undergo significant plastic deformation before rupture, thus hold potential as energy absorbing structural elements subject to high intensity impulsive loads (Amini

* Corresponding author. Tel.: +1 301 405 0364; fax: +1 301 314 9477.

E-mail address: LiT@umd.edu (T. Li).

and Nemat-Nasser, 2010; Amini et al., 2010; Morales et al., 2011; Xue et al., 2008; Xue and Hutchinson, 2007, 2008; Zhang et al., 2009).

Ductile failure of metal layers under in-plane loading often initiates from strain localization, such as the onset of necking instability (Benallal and Tvergaard, 1995; Brunet and Morestin, 2001; Franz et al., 2013; Franz et al., 2009; Haddag et al., 2009; Hashiguchi and Protasov, 2004; Needleman and Tvergaard, 1977; Neil and Agnew, 2009; Tvergaard et al., 1981; Zhang and Wang, 2012). When a metal layer is subject to modest in-plane loading, it deforms uniformly. When the loading increases to a sufficiently high level, the uniform deformation of the metal layer becomes unstable. In other words, infinitesimal perturbation of the metal layer (e.g., non-uniform thickness or pre-existing defects in the metal layer) starts to grow in amplitude, leading to decreasing thickness (i.e., local thinning or necking) in certain locations of the metal layer. On one hand, the metal layer hardens under plastic deformation (i.e., material hardening); on the other hand, local thinning leads to increased stress level at necking locations (i.e., geometric softening). When the geometric softening prevails over material hardening, the onset of necking instability in a material occurs, as attributed to Considere (1885). Localized strain in the necked region promotes the increase of stress triaxiality, which in turn causes microscopic damage and eventually leads to ductile fracture near the neck. For a substrate-supported metal layer under in-plane loading, the critical loading level for necking instability depends on the loading ratio, mechanical properties of both metal and substrate (e.g., effective incremental modulus of the metal/substrate bilayer), the metal/substrate thickness ratio, as well as the orientation of the necking band. For a given substrate-supported metal layer under a certain in-plane loading ratio, necking occurs along a certain orientation that corresponds to the lowest critical loading level. Under tension, plastics neck but the incipient strain localization often gives way to stable neck propagation along the length of the plastic layer. In other words, plastics often harden more than metals. Furthermore, many elastomers can sustain substantial stretch without suffering from necking instability, that is, these elastomers stiffen so steeply that their incremental modulus remains constant or even increases modestly upon tension. By contrast, the incremental modulus of a metal layer decreases monotonically with stretching. Consequently, under tension, a plastic/metal or elastomer/metal bilayer has a greater effective incremental modulus than a single freestanding metal layer. As a result, onset of necking instability in such substrate-supported metal layers is expected to occur at higher strains (Li et al., 2005a; Li and Suo, 2006; Xue and Hutchinson, 2007). Uniaxial tensile experiments have shown that a free-standing thin metal film usually ruptures at a small strain (Espinosa et al., 2003; Huang and Spaepen, 2000; Keller et al., 1996; Nicola et al., 2006; Pashley, 1960; Xiang et al., 2005a). By contrast, plastic-supported thin metal films can sustain tensile strains up to 50% before rupture (Alaca et al., 2002; Chiu et al., 1994; Hommel and Kraft, 2001; Lu et al., 2010; Lu et al., 2007; Macionczyk and Bruckner, 1999; Niu et al., 2007; Xiang et al., 2005b; Yu and Spaepen, 2004). It is predicted that the substrate constraint to the necking development in the metal layer disappears when the metal layer debonds from the substrate (Li et al., 2005a; Li and Suo, 2007), which has been recently verified by the experimental observation of interfacial delamination in the later stage of the tensile fracture process of a thin Cu film on a polyimide substrate (Lu et al., 2007). Necking in a single freestanding metal layer can also be retarded under dynamic stretching due to inertia effect (Guduru and Freund, 2002; Mercier et al., 2010; Mercier and Molinari, 2003; Shenoy and Freund, 1999; Sorensen and Freund, 2000; Xue et al., 2008; Zhang and Ravi-Chandar, 2006). The interaction of the substrate and inertia effects on necking retardation has also been investigated (Amini and Nemat-Nasser, 2010; Amini et al., 2010; Morales et al., 2011; Xue and Hutchinson, 2007, 2008; Zhang et al., 2009).

In practice, substrate-supported metal layers are often subject to large and complicated in-plane loading. For example, the electronic sensitive skins covering the elbow of a robot experience large biaxial stretches. The understanding of necking instability of substrate-supported metal layers under arbitrary biaxial in-plane loading, however, is poorly studied so far. Most existing theoretical studies assume plane strain condition of the bilayer deformation. Xue and Hutchinson (2007) investigated the necking retardation of elastomer-supported metal layers under biaxial loading, but the biaxial loading ratio in that study is limited to be in the positive regime. As to be shown later in the present paper, in the positive loading ratio regime, the necking band always occurs in the direction perpendicular to that of the greater tensile load. By contrast, most reported tensile experiments of substrate-supported metal layers are uniaxial tests. As commonly observed in such uniaxial tensile experiments, the incipient necking bands often occur along a slanted direction in between the two loading directions. For example, Fig. 1a shows the necking bands in a thin Cu film (170 nm thick) supported by a polyimide substrate (100 μm thick) occur along a direction about 60° away from the uniaxial loading direction. Similar experimental results showing inclined necking bands have also been reported recently (Lu et al., 2010; Macionczyk and Bruckner, 1999; Gruber et al., 2004). So far, the quantitative correlation between the necking limit strain as well as the necking band orientation and the material properties and thickness ratio of a metal/substrate bilayer in the full range of biaxial in-plane loading ratio still remains unclear.

This paper presents a comprehensive investigation to decipher the above quantitative correlation in two representative material structures, namely, a metal layer supported by a stiff plastic substrate, and a metal layer supported by a compliant elastomer substrate, respectively. In particular, bifurcation analysis predicts that a metal layer supported by a sufficiently stiff and thick elastomer substrate is immune from long wavelength necking instability. This further motivates the investigation of the enhanced energy absorption and dissipation of an elastomer-supported metal layer in comparison with that of an all-metal single layer with the same mass. It is noted that the necking limit analysis in the present study is based on a bifurcation analysis at the long-wavelength limit. In other words, such a necking instability later leads to a single localized neck in an infinitely large substrate-supported metal layer. In reality, other types of deformation instability (e.g., multiple diffusive necks or surface instability) could appear upon the onset of failure in substrate-supported metal layers, the study

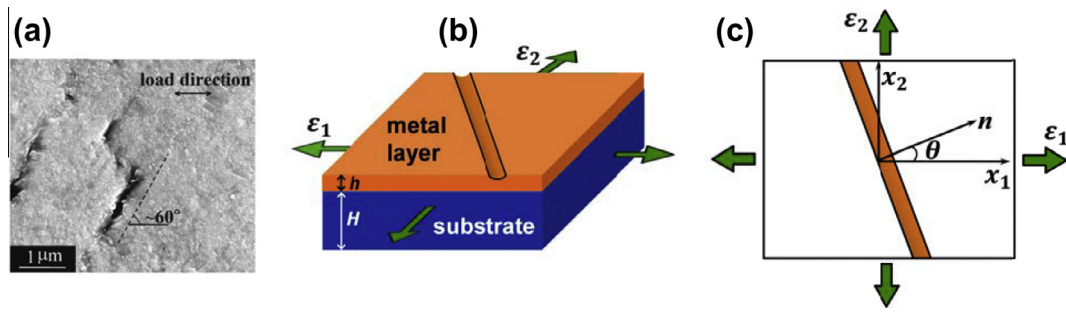


Fig. 1. (a) When a copper film (170 nm thick) supported by a polyimide substrate (100 μm thick) is subject to uniaxial tension, necking bands occur along a direction about 60° away from the loading direction. (b) Schematic of necking formation in a substrate-supported metal layer under biaxial in-plane loading. (c) Top view of the substrate-supported metal layer with a necking band oriented in between the two in-plane loading directions.

of which is beyond the scope of this paper and will be reported elsewhere. Further discussion in this regard is presented in Section 4.

2. Mechanics model

2.1. Constitutive relations

Necking instability occurs at strains sufficiently large so that the elasticity of the metal layer can be neglected. In this study, we describe the constitutive relation of metal using the finite strain J_2 deformation theory of plasticity developed by Hill (1970) and Hutchinson and Neale (1978), as recapped below. With reference to Cartesian base vectors coaxial with the principal stress axes, we have

$$\bar{\sigma}_{ij} = L_{ijkl} \dot{\epsilon}_{kl} + \dot{p} \delta_{ij} \tag{1}$$

where $\bar{\sigma}_{ij}$ is the Jaumann rate of the Cauchy stress, $\dot{\epsilon}_{ij}$ is the Eulerian strain rate, \dot{p} is the hydrostatic part of the stress rate (Hereinafter, $\bar{\cdot}$ denotes objective Jaumann rates, while $\dot{\cdot}$ denotes time rates), and δ_{ij} is the Kronecker delta. The instantaneous moduli L_{ijkl} are assumed to satisfy the indicial symmetries

$$L_{ijkl} = L_{jikl} = L_{ijlk} = L_{klij} \tag{2}$$

Let σ_{ij} be the Cauchy stress, s_{ij} be the deviatoric stress and $\sigma_e = \sqrt{3s_{ij}s_{ij}/2}$ be the effective stress; then the instantaneous moduli can be given as

$$L_{ijkl} = \frac{2}{3} E_s \left[\frac{1}{2} (\delta_{ik} \delta_{jl} + \delta_{jk} \delta_{il}) - \frac{1}{3} \delta_{ij} \delta_{kl} \right] - (E_s - E_t) \frac{s_{ij} s_{kl}}{\sigma_e^2} + Q_{ijkl} \tag{3}$$

where E_s and E_t are the secant modulus and tangent modulus of the uniaxial true stress-Eulerian strain curve at σ_e , respectively. For Q_{ijkl} , the last term in (3), its only non-zero components in principal axes are the “shearing” terms, such as

$$Q_{1212} = \frac{1}{3} E_s [(\epsilon_1 - \epsilon_2) \coth(\epsilon_1 - \epsilon_2) - 1] \tag{4}$$

Notice that in (4), $\epsilon_1 = \epsilon_{11}$ and $\epsilon_2 = \epsilon_{22}$, as the Cartesian base vectors are coaxial with the principal Eulerian strains.

In view of the above remarks, by using the definition of L_{ijkl} and the incompressibility condition $\dot{\epsilon}_{kk} = 0$, the constitutive law (1) can be expressed as

$$\bar{\sigma}_{ij} = \frac{2}{3} E_s \dot{\epsilon}_{ij} - (E_s - E_t) \frac{s_{ij} s_{kl}}{\sigma_e^2} \dot{\epsilon}_{kl} + Q_{ijkl} \dot{\epsilon}_{kl} + \dot{p} \delta_{ij} \tag{5}$$

In the localized necking band analysis, plane stress condition is assumed. The plane stress assumption has been shown to be valid for long wavelength necking limit analysis (Hutchinson et al., 1978). Before necking instability occurs, the only two non-vanishing stress components are $\sigma_{11} = \sigma_1$ and $\sigma_{22} = \sigma_2$ ($\sigma_{33} = 0$). Taking advantage of the plane stress condition $\bar{\sigma}_{33} = 0$ and the incompressibility condition, the hydrostatic stress rate \dot{p} can be solved as

$$\dot{p} = \left(\frac{2}{3} E_s \dot{\epsilon}_{11} + \frac{2}{3} E_s \dot{\epsilon}_{22} \right) + (E_s - E_t) \frac{s_{33}}{\sigma_e^2} [\sigma_{11} \dot{\epsilon}_{11} + \sigma_{22} \dot{\epsilon}_{22}] \tag{6}$$

Substituting (6) into (1), the constitutive relation (1) can be reduced to

$$\bar{\sigma}_1 = L_{11} \dot{\epsilon}_1 + L_{12} \dot{\epsilon}_2 \tag{7}$$

$$\bar{\sigma}_2 = L_{21} \dot{\epsilon}_1 + L_{22} \dot{\epsilon}_2 \tag{8}$$

$$\bar{\sigma}_{12} = 2L_s \dot{\varepsilon}_{12} \quad (9)$$

where the instantaneous moduli $L_{ij}(i, j = 1, 2)$ are given by

$$L_{11} = \frac{4}{3}E_s - (E_s - E_t) \left(\frac{\sigma_1}{\sigma_e} \right)^2 \quad (10)$$

$$L_{22} = \frac{4}{3}E_s - (E_s - E_t) \left(\frac{\sigma_2}{\sigma_e} \right)^2 \quad (11)$$

$$L_{12} = L_{21} = \frac{2}{3}E_s - (E_s - E_t) \frac{\sigma_1 \sigma_2}{\sigma_e^2} \quad (12)$$

$$L_s = \frac{1}{3}E_s(\varepsilon_1 - \varepsilon_2) \coth(\varepsilon_1 - \varepsilon_2) = \frac{1}{3}E_s(\varepsilon_1 - \varepsilon_2) \frac{e^{2\varepsilon_1} + e^{2\varepsilon_2}}{e^{2\varepsilon_1} - e^{2\varepsilon_2}} \quad (13)$$

J_2 deformation theory gives the relation between the principal Eulerian strain and the principal deviatoric stress as follows

$$\varepsilon_i = \mu s_i, \quad (14)$$

where μ can be obtained from the uniaxial tension curve and is a function of the effective stress $\sigma_e = \sqrt{3s_i s_i / 2}$ and the effective strain $\varepsilon_e = \sqrt{2\varepsilon_i \varepsilon_i / 3}$. Therefore,

$$\mu = \frac{3}{2} \frac{\varepsilon_e}{\sigma_e} = \frac{3}{2E_s} \quad (15)$$

Imposing proportional straining path

$$\frac{\varepsilon_2}{\varepsilon_1} = \rho = \text{constant} \quad (16)$$

to the structure, we then have

$$\sigma_1 = \frac{2E_s}{3}(2 + \rho)\varepsilon_1 \quad (17)$$

$$\sigma_2 = \frac{2E_s}{3}(1 + 2\rho)\varepsilon_1 \quad (18)$$

$$\sigma_e = \frac{2E_s}{3} \sqrt{3(1 + \rho + \rho^2)}\varepsilon_1 \quad (19)$$

For a material with a power-law hardening $\sigma_e = K\varepsilon_e^N$ in the plastic range, the secant modulus and tangent modulus can be given by

$$E_s = K\varepsilon_e^{N-1} \quad (20)$$

$$E_t = NK\varepsilon_e^{N-1}, \quad (21)$$

respectively, where

$$\varepsilon_e = 2\sqrt{\frac{1 + \rho + \rho^2}{3}}\varepsilon_1 \quad (22)$$

The above constitutive relation is also adopted in this study to describe the stress–strain behavior of the stiff plastic substrate.

The elastomer substrate in this study is described as incompressible neo-Hookean materials, whose strain energy density W is given by

$$W = \frac{E}{6}(\lambda_1^2 + \lambda_2^2 + \lambda_3^2 - 3) \quad (23)$$

where E is Young's modulus at zero strain, $\lambda_i(i = 1-3)$ are the principal stretches. The incompressibility implies a constraint that $\lambda_1 \lambda_2 \lambda_3 = 1$. As a result of the plane stress condition $\sigma_{33} = 0$, we have

$$\sigma_1 \equiv \sigma_{11} = \frac{E}{3}(\lambda_1^2 - \lambda_3^2) = \frac{E}{3}[e^{2\varepsilon_1} - e^{-2(\varepsilon_1 + \varepsilon_2)}] \quad (24)$$

$$\sigma_2 \equiv \sigma_{22} = \frac{E}{3}(\lambda_2^2 - \lambda_3^2) = \frac{E}{3}[e^{2\varepsilon_2} - e^{-2(\varepsilon_1 + \varepsilon_2)}]. \quad (25)$$

All shear stress components vanish given the proportional loading path. Following Biot (Biot, 1965), the rate form of constitutive relation for Neo-Hookean material can be given as follows

$$\bar{\sigma}_{11} = \frac{4E}{9} \lambda_1^2 \dot{\epsilon}_1 - \frac{2E}{9} \lambda_2^2 \dot{\epsilon}_2 - \frac{2E}{9} \lambda_3^2 \dot{\epsilon}_3 + \dot{p} \quad (26)$$

$$\bar{\sigma}_{22} = -\frac{2E}{9} \lambda_1^2 \dot{\epsilon}_1 + \frac{4E}{9} \lambda_2^2 \dot{\epsilon}_2 - \frac{2E}{9} \lambda_3^2 \dot{\epsilon}_3 + \dot{p} \quad (27)$$

$$\bar{\sigma}_{33} = -\frac{2E}{9} \lambda_1^2 \dot{\epsilon}_1 - \frac{2E}{9} \lambda_2^2 \dot{\epsilon}_2 + \frac{4E}{9} \lambda_3^2 \dot{\epsilon}_3 + \dot{p} \quad (28)$$

$$\bar{\sigma}_{12} = \frac{E}{3} (\lambda_1^2 + \lambda_2^2) \dot{\epsilon}_{12} \quad (29)$$

Take advantage of the plane stress condition $\bar{\sigma}_{33} = 0$, the hydrostatic stress rate \dot{p} can be explicitly solved as

$$\dot{p} = \frac{2E}{9} \lambda_1^2 \dot{\epsilon}_1 + \frac{2E}{9} \lambda_2^2 \dot{\epsilon}_2 - \frac{4E}{9} \lambda_3^2 \dot{\epsilon}_3 \quad (30)$$

Substitute (30) into (26) and (27) and consider the incompressibility $\dot{\epsilon}_1 + \dot{\epsilon}_2 + \dot{\epsilon}_3 = 0$, the rate-form constitutive relation for the neo-Hookean material can be written in a more compact way similar to (7–9) as follows

$$\bar{\sigma}_1 = \hat{L}_{11} \dot{\epsilon}_1 + \hat{L}_{12} \dot{\epsilon}_2 \quad (31)$$

$$\bar{\sigma}_2 = \hat{L}_{21} \dot{\epsilon}_1 + \hat{L}_{22} \dot{\epsilon}_2 \quad (32)$$

$$\bar{\sigma}_{12} = 2\hat{L}_s \dot{\epsilon}_{12} \quad (33)$$

where the explicit form of instantaneous moduli $\hat{L}_{ij} (i, j = 1, 2)$ is given by

$$\hat{L}_{11} = \frac{2E}{3} [\lambda_1^2 + \lambda_2^2] = \frac{2E}{3} [e^{2\epsilon_1} + e^{-2(\epsilon_1 + \epsilon_2)}] \quad (34)$$

$$\hat{L}_{22} = \frac{2E}{3} [\lambda_2^2 + \lambda_3^2] = \frac{2E}{3} [e^{2\epsilon_2} + e^{-2(\epsilon_1 + \epsilon_2)}] \quad (35)$$

$$\hat{L}_{12} = \hat{L}_{21} = \frac{2E}{3} \lambda_3^2 = \frac{2E}{3} e^{-2(\epsilon_1 + \epsilon_2)} \quad (36)$$

$$\hat{L}_s = \frac{E}{6} (\lambda_1^2 + \lambda_2^2) = \frac{E}{6} (e^{2\epsilon_1} + e^{2\epsilon_2}) \quad (37)$$

2.2. Localized necking analysis for a substrate-supported metal layer under in-plane loading

Consider a flat metal layer of uniform initial thickness h perfectly adhered to a substrate of uniform initial thickness H (Fig. 1b). The metal/substrate bilayer is subject to a homogeneous strain field with in-plane strains $\epsilon_{11}^s = \epsilon_{11}^m = \epsilon_1$, $\epsilon_{22}^s = \epsilon_{22}^m = \epsilon_2$ and all other $\epsilon_{ij} = 0 (i \neq j)$. Here, the superscripts m and s denote the metal and substrate, respectively. Therefore, the stress field is also homogeneous per zone with $\sigma_{11}^{m(s)} = \sigma_1^{m(s)}$, $\sigma_{22}^{m(s)} = \sigma_2^{m(s)}$ and all other $\sigma_{ij}^{m(s)} = 0$ before necking instability occurs. Under a proportional loading path (i.e., $\epsilon_2/\epsilon_1 = \rho$), the bilayer first deforms homogeneously, and above a critical strain level, homogeneous deformation gives way to strain localization in the form of localized plastic deformation in a narrow band which is referred as the necking band while the deformation remains homogeneous elsewhere. The necking band sets in with its in-plane normal direction \mathbf{n} making an inclination angle θ to x_1 direction (Fig. 1c).

The bifurcation analysis of a freestanding metal sheet (Hill and Hutchinson, 1975; Hutchinson and Neale, 1978; Storen and Rice, 1975) is adapted to study the necking limit of a substrate-supported metal layer. We assume the plastic flow field within the necking band varies across the band along its normal direction, i.e.,

$$\Delta v_i = v_{i,inside} - v_{i,outside} = F_i (n_1 x_1 + n_2 x_2) \quad i = 1, 2 \quad (38)$$

where $v_{i,inside} (i = 1, 2)$ is the velocity components in the necking band and $v_{i,outside}$ is the linear continuation of the outside velocity field through the necking band. Δv_i denotes the differences between the velocity components inside and outside the necking band and it vanishes at boundary of necking band to make velocity field remain continuous, and $n_1 = \cos\theta$ and $n_2 = \sin\theta$ are the components of the unit normal to the necking band (Fig. 1c). Then the velocity gradients within the necking band can be written as

$$\Delta v_{i,j} = F'_i n_j \equiv f_i n_j \quad i, j = 1, 2 \quad (39)$$

Accordingly, the strain rate field inside the necking band is given by

$$\dot{\varepsilon}_{ij} = \frac{1}{2}(\Delta v_{ij} + \Delta v_{j,i}) \quad i, j = 1, 2 \quad (40)$$

Incompressibility of total deformation gives that $\dot{\varepsilon}_{33} = -(\dot{\varepsilon}_{11} + \dot{\varepsilon}_{22})$.

At the onset of necking, equilibrium across the necking band and its underlying substrate part requires that the nominal traction rates \dot{T}_i on the necking band boundaries be continuous. Thus,

$$\Delta \dot{T}_j^m h + \Delta \dot{T}_j^s H = n_i \dot{t}_{ij}^m h + n_i \dot{t}_{ij}^s H = 0 \quad (41)$$

where \dot{t}_{ij} is the difference between the nominal stress rate components inside and outside the necking band. Superscripts m and s denote the metal layer and the substrate, respectively. \dot{t}_{ij} can be related to the Jaumann rate of the Cauchy stress $\bar{\sigma}_{ij}$ through

$$\dot{t}_{ij} = \bar{\sigma}_{ij} + \sigma_{ik} \Delta v_{j,k} - (\sigma_{ik} \dot{\varepsilon}_{jk} + \sigma_{jk} \dot{\varepsilon}_{ik}) \quad (42)$$

Substituting (42) and the constitutive relations presented in Section 2.1 into the equilibrium Eq. (41), a set of linear homogeneous equations in f_1 and f_2 can be obtained as follows,

$$\begin{bmatrix} g_{11} & g_{12} \\ g_{21} & g_{22} \end{bmatrix} \begin{bmatrix} f_1 \\ f_2 \end{bmatrix} = \begin{bmatrix} 0 \\ 0 \end{bmatrix} \quad (43)$$

where

$$g_{11} = \left\{ n_1^2 (L_{11}^m - \sigma_1^m) + n_2^2 \left[L_s^m + \frac{1}{2} (\sigma_2^m - \sigma_1^m) \right] \right\} h + \left\{ n_1^2 (L_{11}^s - \sigma_1^s) + n_2^2 \left[L_s^s + \frac{1}{2} (\sigma_2^s - \sigma_1^s) \right] \right\} H \quad (44)$$

$$g_{12} = g_{21} = n_1 n_2 \left[L_{12}^m + L_s^m - \frac{1}{2} (\sigma_1^m + \sigma_2^m) \right] h + n_1 n_2 \left[L_{12}^s + L_s^s - \frac{1}{2} (\sigma_1^s + \sigma_2^s) \right] H \quad (45)$$

$$g_{22} = \left\{ n_1^2 \left[L_s^m + \frac{1}{2} (\sigma_1^m - \sigma_2^m) \right] + n_2^2 (L_{22}^m - \sigma_2^m) \right\} h + \left\{ n_1^2 \left[L_s^s + \frac{1}{2} (\sigma_1^s - \sigma_2^s) \right] + n_2^2 (L_{22}^s - \sigma_2^s) \right\} H. \quad (46)$$

The condition for the onset of necking instability is met if non-trivial solution of f_1 and f_2 exists to satisfy (43). That is,

$$\det \begin{bmatrix} g_{11} & g_{12} \\ g_{21} & g_{22} \end{bmatrix} = 0 \quad (47)$$

For a metal layer with a power-law hardening $\sigma_e = K_m \varepsilon_e^{N_m}$ supported by a plastic substrate with a power-law hardening $\sigma_e = K_s \varepsilon_e^{N_s}$, (47) becomes

$$\begin{aligned} & \left\{ \left\{ \cos^2 \theta \left[4 - (1 - N_m) \frac{(2 + \rho)^2}{(1 + \rho + \rho^2)} - 2(2 + \rho) \varepsilon_1 \right] + \sin^2 \theta \left[(1 - \rho) \frac{2}{e^{2(1-\rho)\varepsilon_1} - 1} \varepsilon_1 \right] \right\} \right. \\ & + S \left\{ \cos^2 \theta \left[4 - (1 - N_s) \frac{(2 + \rho)^2}{(1 + \rho + \rho^2)} - 2(2 + \rho) \varepsilon_1 \right] + \sin^2 \theta \left[(1 - \rho) \frac{2}{e^{2(1-\rho)\varepsilon_1} - 1} \varepsilon_1 \right] \right\} \left(\frac{2\sqrt{1 + \rho + \rho^2} \varepsilon_1}{\sqrt{3}} \right)^{N_s - N_m} \left. \right\} \\ & * \left\{ \left\{ \cos^2 \theta \left[(1 - \rho) \frac{2e^{2(1-\rho)\varepsilon_1}}{e^{2(1-\rho)\varepsilon_1} - 1} \varepsilon_1 \right] + \sin^2 \theta \left[4 - (1 - N_m) \frac{(1 + 2\rho)^2}{(1 + \rho + \rho^2)} - 2(1 + 2\rho) \varepsilon_1 \right] \right\} \right. \\ & + S \left\{ \cos^2 \theta \left[(1 - \rho) \frac{2e^{2(1-\rho)\varepsilon_1}}{e^{2(1-\rho)\varepsilon_1} - 1} \varepsilon_1 \right] + \sin^2 \theta \left[4 - (1 - N_s) \frac{(1 + 2\rho)^2}{(1 + \rho + \rho^2)} - 2(1 + 2\rho) \varepsilon_1 \right] \right\} \left(\frac{2\sqrt{1 + \rho + \rho^2} \varepsilon_1}{\sqrt{3}} \right)^{N_s - N_m} \left. \right\} \\ & - \cos^2 \theta \sin^2 \theta \left\{ \left[2 - (1 - N_m) \frac{(1 + 2\rho)(2 + \rho)}{1 + \rho + \rho^2} + (1 - \rho) \frac{e^{2(1-\rho)\varepsilon_1} + 1}{e^{2(1-\rho)\varepsilon_1} - 1} \varepsilon_1 - 3(1 + \rho) \varepsilon_1 \right] \right. \\ & \left. + S \left[2 - (1 - N_s) \frac{(1 + 2\rho)(2 + \rho)}{1 + \rho + \rho^2} + (1 - \rho) \frac{e^{2(1-\rho)\varepsilon_1} + 1}{e^{2(1-\rho)\varepsilon_1} - 1} \varepsilon_1 - 3(1 + \rho) \varepsilon_1 \right] \left(\frac{2\sqrt{1 + \rho + \rho^2} \varepsilon_1}{\sqrt{3}} \right)^{N_s - N_m} \right\}^2 = 0, \quad (48) \end{aligned}$$

where dimensionless group $S = (K_s H) / (K_m h)$.¹

¹ Hereinafter, for a plastic-supported metal layer, N_m and N_s denote the hardening index of the power-law metal and plastic substrate, respectively; for a neo-Hookean elastomer-supported metal layer or a freestanding metal layer, N is used to denote the hardening index of the power-law metal.

For a given value of ρ , critical strains ε_1 can be solved numerically from (48) in the permissible range of inclination angle θ (between 0° and 90°). The lowest critical strain and the corresponding angle define the necking limit strain and the necking band orientation of a plastic-supported metal layer under a biaxial loading ratio ρ , respectively.

For a power law metal layer supported by a neo-Hookean elastomer substrate, (47) becomes

$$\left\{ \left\{ \cos^2 \theta \left[4 - (1 - N) \frac{(2 + \rho)^2}{(1 + \rho + \rho^2)} - 2(2 + \rho)\varepsilon_1 \right] + \sin^2 \theta \left[(1 - \rho) \frac{2}{e^{2(1-\rho)\varepsilon_1} - 1} \varepsilon_1 \right] \right\} \left(\frac{2\sqrt{1 + \rho + \rho^2}\varepsilon_1}{\sqrt{3}} \right)^{N-1} + S \left\{ \cos^2 \theta [e^{2\varepsilon_1} + 3e^{-2(1+\rho)\varepsilon_1}] + \sin^2 \theta e^{2\rho\varepsilon_1} \right\} * \left\{ \cos^2 \theta \left[(1 - \rho) \frac{2e^{2(1-\rho)\varepsilon_1}}{e^{2(1-\rho)\varepsilon_1} - 1} \varepsilon_1 \right] + \sin^2 \theta \left[4 - (1 - N) \frac{(1 + 2\rho)^2}{(1 + \rho + \rho^2)} - 2(1 + 2\rho)\varepsilon_1 \right] \right\} \left(\frac{2\sqrt{1 + \rho + \rho^2}\varepsilon_1}{\sqrt{3}} \right)^{N-1} + S \left\{ \cos^2 \theta e^{2\varepsilon_1} + \sin^2 \theta [e^{2\rho\varepsilon_1} + 3e^{-2(1+\rho)\varepsilon_1}] \right\} \right\} - \left\{ \cos^2 \theta \left[(1 - \rho) \frac{2e^{2(1-\rho)\varepsilon_1}}{e^{2(1-\rho)\varepsilon_1} - 1} \varepsilon_1 \right] + \sin^2 \theta \left[4 - (1 - N) \frac{(1 + 2\rho)^2}{(1 + \rho + \rho^2)} - 2(1 + 2\rho)\varepsilon_1 \right] \right\} \left(\frac{2\sqrt{1 + \rho + \rho^2}\varepsilon_1}{\sqrt{3}} \right)^{N-1} + S \left\{ \cos^2 \theta e^{2\varepsilon_1} + \sin^2 \theta [e^{2\rho\varepsilon_1} + 3e^{-2(1+\rho)\varepsilon_1}] \right\} - \cos^2 \theta \sin^2 \theta \left\{ \left[2 - (1 - N) \frac{(1 + 2\rho)(2 + \rho)}{1 + \rho + \rho^2} + (1 - \rho) \frac{e^{2(1-\rho)\varepsilon_1} + 1}{e^{2(1-\rho)\varepsilon_1} - 1} \varepsilon_1 - 3(1 + \rho)\varepsilon_1 \right] \times \left(\frac{2\sqrt{1 + \rho + \rho^2}\varepsilon_1}{\sqrt{3}} \right)^{N-1} + 3Se^{-2(1+\rho)\varepsilon_1} \right\}^2 = 0, \tag{49}$$

where dimensionless group $S = (EH)/(K_m h)$.

Similarly, the necking limit strain and necking band orientation of the elastomer-supported metal layer under a biaxial loading ratio ρ can be defined as the lowest possible critical strain satisfying (49) and its corresponding inclination angle θ , respectively.

3. Results and discussion

3.1. Necking limit of freestanding metal layers under biaxial in-plane loading

We first present the representative results from necking instability analysis of freestanding metal layers as a demonstration of the dependence of necking limit strain and necking band orientation on biaxial in-plane loading. Similar studies have been well reported in previous literature (e.g., Hill and Hutchinson (1975), Hutchinson and Neale (1978), Storen and Rice (1975)).

The governing equation of the necking limit of a freestanding metal layer can be readily obtained by reducing (48) or (49) using $S = 0$. Fig. 2 plots the critical strain of the onset of necking instability in a freestanding metal layer as a function of necking band inclination angle θ , for three representative in-plane loading conditions, i.e., equibiaxial tension ($\rho = 1$), plane-strain tension ($\rho = 0$) and uniaxial tension $\rho = -1/2$.

Under equibiaxial tension, the critical necking condition (48) reduces to

$$S(e^{2\varepsilon_1} + 3e^{-4\varepsilon_1}) - (1 + 3N - 6\varepsilon_1)(2\varepsilon_1)^{N-1} = 0, \tag{50}$$

which agrees with the results in Xue and Hutchinson (2007). Note that such a condition is independent of the necking band inclination angle θ (Fig. 2a). In other words, under equibiaxial tension, necking instability could occur in any orientation if

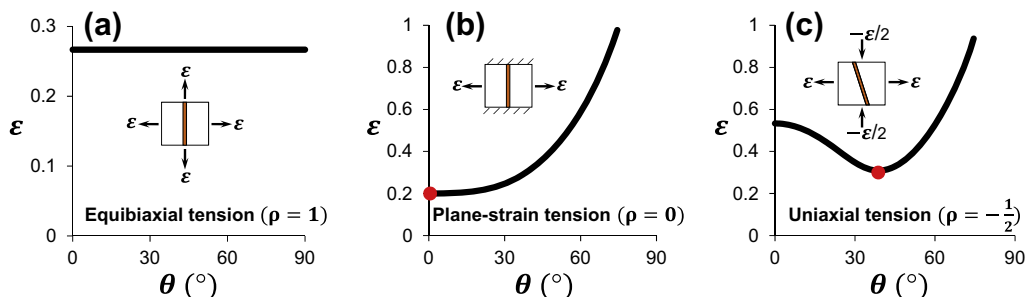


Fig. 2. Critical necking limit strain ε of a freestanding metal layer as a function of inclination angle of the necking band θ when the layer is under three representative types of in-plane loading. Here the hardening index of the metal layer $N = 0.2$. (a) Under equibiaxial tension, necking instability could occur in any orientation at a critical necking strain $\varepsilon = \frac{1+3N}{6} \cong 0.27$; (b) Under plane-strain tension, the lowest critical necking strain $\varepsilon = N = 0.2$, and necking instability occurs along the direction perpendicular to the applied tension (i.e., $\theta = 0^\circ$); (c) Under uniaxial tension, however, the lowest critical necking strain $\varepsilon = 0.31$, and necking instability occurs along a direction of $\theta = 39^\circ$.

the applied loading reaches the necking limit strain determined by (50). For a freestanding metal layer, i.e., $S = 0$, (50) further reduces to

$$\varepsilon_1 = \frac{1 + 3N}{6}. \quad (51)$$

This means that the necking limit strain of a freestanding metal layer with power-law hardening under equibiaxial tension depends only on its hardening index.

Under plane-strain tension, the lowest critical strain of the onset of necking instability in a freestanding metal layer always occurs when $\theta = 0$, as shown in Fig. 2b. That is, necking band always appears along the direction perpendicular to the plane-strain tension direction. The critical necking limit strain reduces to the well-known Considere criterion

$$\varepsilon_1 = N. \quad (52)$$

By contrast, as shown in Fig. 2c, under uniaxial tension, the lowest critical strain of the onset of necking instability in a freestanding metal layer occurs at a finite value of θ . That is, necking band appears along a slanted direction to the uniaxial tension direction. For example, for a hardening index of $N = 0.2$, the necking limit strain under uniaxial tension is 0.31, with a necking band inclination angle of about 39° .

3.2. Necking limit of plastic-supported metal layers under biaxial in-plane loading

The necking limit of a plastic/metal bilayer depends on four parameters: the loading ratio ρ , the hardening indices of the metal N_m and of the substrate N_s , and a dimensionless group $S = (K_s H)/(K_m h)$. Fig. 3a and c plot the combinations of the two in-plane strain components ε_1 and ε_2 at the onset of the necking instability of a plastic-supported metal layer, for two different combinations of N_m and N_s . The necking limit diagrams such as those shown in Fig. 3a and c and later in Fig. 4a, c,

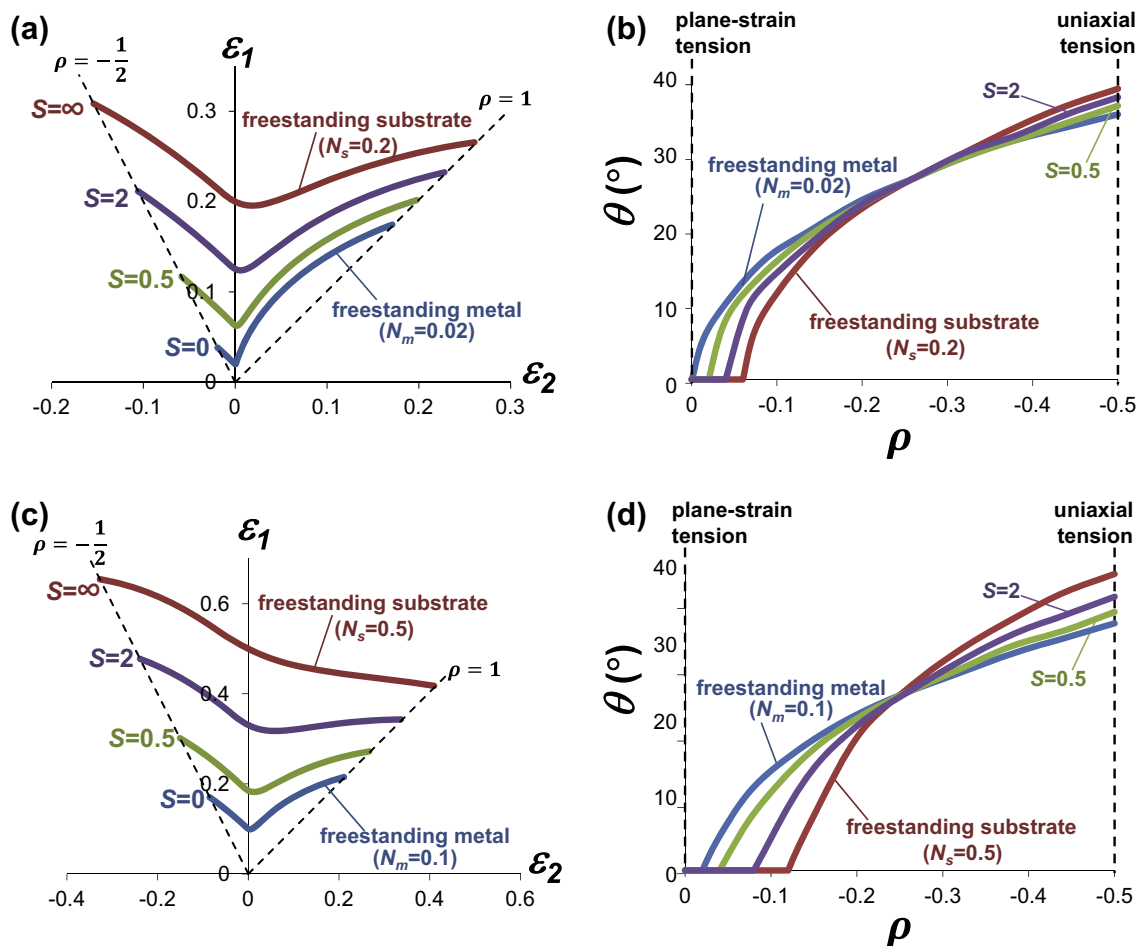


Fig. 3. Necking limit curves showing strains at the onset of necking in a plastic-supported metal layer as a function of $S = (K_s H)/(K_m h)$. (a) $N_m = 0.02, N_s = 0.2$. (c) $N_m = 0.1, N_s = 0.5$. (b) and (d) plot the corresponding necking band inclination angle θ as a function of negative loading ratio ρ .

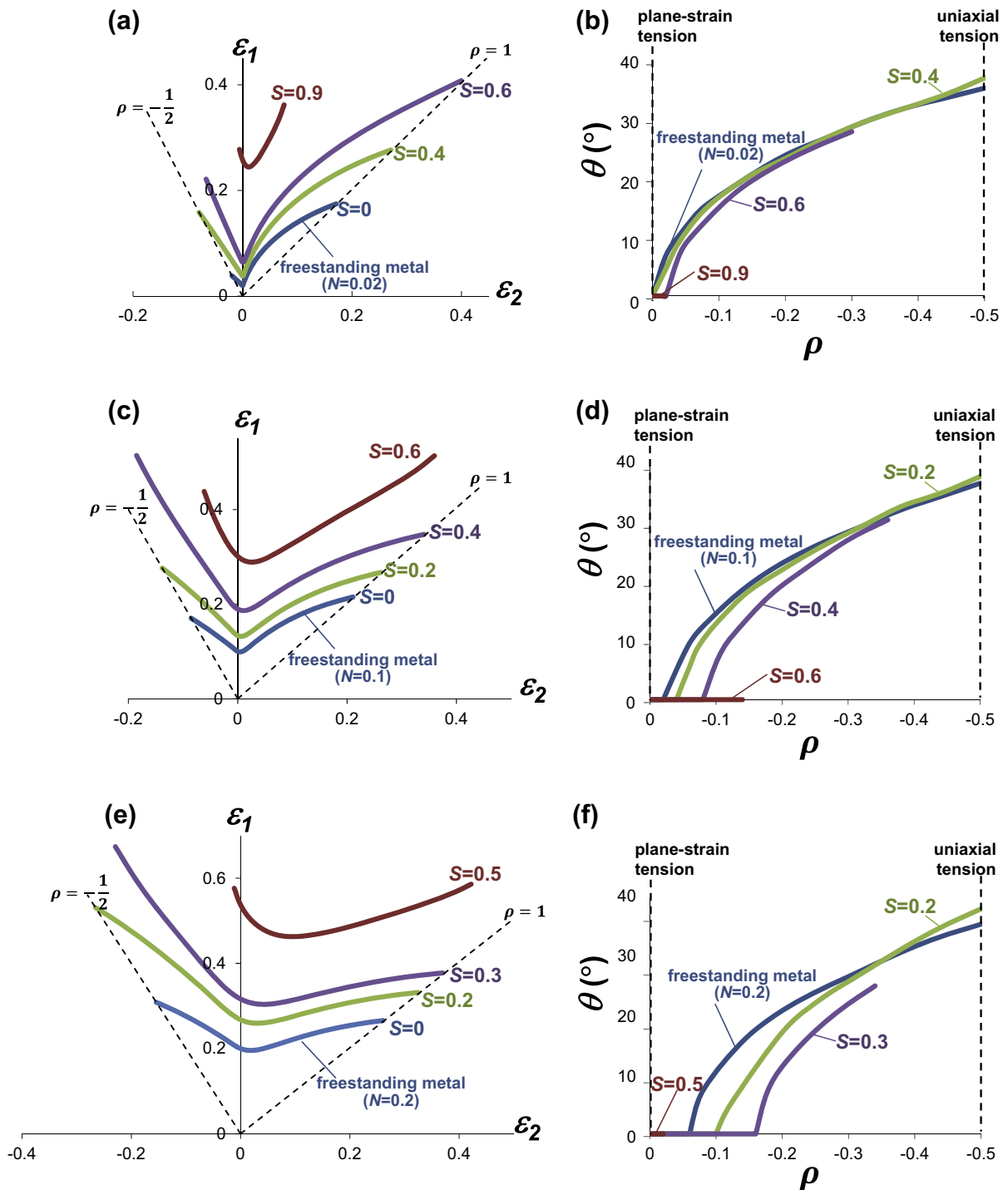


Fig. 4. Necking limit curves showing strains at the onset of necking in an elastomer-supported metal film as a function of $S = (EH)/(K_m h)$. (a) $N = 0.02$. (c) $N = 0.1$, (e) $N = 0.2$. (b), (d) and (f) plot the corresponding necking band inclination angle θ as a function of negative loading ratio ρ .

e, are analogous to the “forming limit diagram” as referred to as in the literature of sheet metal forming (Barlat, 1987; Hashiguchi and Protasov, 2004; Kuroda and Tvergaard, 2000; Marciniak et al., 1973; Stoughton, 2000; Zhang and Wang, 2012; Zhao et al., 1996), and can serve as guidelines in designing functional substrate-supported metal layers of certain desirable deformability.

Fig. 3a shows four necking limit curves corresponding to $S = 0, 0.5, 2$ and ∞ , respectively. Here, $N_m = 0.02$ and $N_s = 0.2$. For each curve, it is evident that the critical necking limit strain ε_1 under plane-strain tension ($\varepsilon_2 = 0$) is lower than those under equibiaxial tension and uniaxial tension. For example, when $S = 0.5$, the critical necking limit strains ε_1 under these three representative biaxial loadings are 0.065, 0.20, and 0.12, respectively. In this sense, previous studies assuming plane-strain condition tend to underestimate the necking limit of the plastic-supported metal layers subject to uniaxial tensile loading. Comparison among the curves in Fig. 3a shows that, for a given loading ratio, the necking limit strain of a plastic-supported metal layer is higher than that of the freestanding metal layer. In other words, the necking is retarded to occur at a higher strain. The larger the value of S , the more significant retardation of necking occurrence. The limiting case of $S = \infty$ corresponds to a freestanding plastic substrate, whose necking limit strains ε_1 are 0.2 (plane-strain), 0.31 (uniaxial) and 0.27 (equibiaxial), respectively. In other words, the effect of the plastic substrate on necking retardation is capped by the necking instability of the substrate itself. Similar necking retardation effect and its dependence on loading ratio ρ and dimensionless group S are evident in Fig. 3c, in which $N_m = 0.1$ and $N_s = 0.5$.

The necking limit analysis shows that, in positive loading ratio regime ($\rho > 0$), the necking band always occurs in the direction perpendicular to that of the greater tensile strain (i.e., $\theta = 0$), while in negative loading ratio regime, the necking band could appear in a slanted direction in between the two loading directions. Fig. 3b plots the necking band inclination angle θ as a function of a negative loading ratio ρ , for $S = 0, 0.5, 2$ and ∞ . Here, $N_m = 0.02$ and $N_s = 0.2$. In a freestanding metal layer, the necking band starts to incline as ρ becomes negative. The inclination angle θ increases as ρ further decreases, which reaches 35.5° when $\rho = -1/2$ (uniaxial tension). In a plastic-supported metal layer, the necking band remains along the smaller tensile loading direction ($\theta = 0$) until a finite negative value of ρ is reached. For example, when $S = 2$, the necking band starts to incline when $\rho < -0.04$. The smaller the loading ratio, the larger the inclination angle. Under uniaxial tension, $\theta = 36.7^\circ$ and 37.8° for $S = 0.5$ and 2 , respectively. Such a prediction of necking band inclination angle agrees reasonably well with the orientation of the necking bands in the polyimide-supported copper film under uniaxial tension (Fig. 1a, note that the $\sim 60^\circ$ angle is complementary with θ). Similar dependence of necking band inclination angle on loading ratio ρ and dimensionless group S is also observed in Fig. 3d, in which $N_m = 0.1$ and $N_s = 0.5$.

3.3. Necking limit of elastomer-supported metal layers under biaxial in-plane loading

The necking limit of an elastomer/metal bilayer depends on three parameters: the loading ratio ρ , the hardening index of the metal N , and a dimensionless group $S = (EH)/(K_m h)$. Fig. 4a, c and e plot the necking limit diagrams of an elastomer-supported metal layer, for three different values of $N = 0.02, 0.1$ and 0.2 , respectively.

Fig. 4a shows four necking limit curves corresponding to $S = 0$ (freestanding metal layer), $0.4, 0.6$, and 0.9 . The dependence of the necking limit strain of the elastomer-supported metal layer on loading ratio is similar to that of plastic-supported metal layers (Fig. 3a and c). The effect of necking retardation becomes more significant as S increases. Interestingly, Fig. 4a reveals that, if S is sufficiently large, there exists certain range of loading ratio, in which the necking limit strain tends to infinity (e.g., when $\rho < -0.3$ if $S = 0.6$, or when $\rho < -0.03$ or $\rho > 0.21$ if $S = 0.9$). Indeed, there exists a critical value of S , above which the necking limit strain tends to infinity in all range of ρ . In other words, when the elastomer substrate is sufficiently stiff and/or thick, the metal layer is immune from necking instability, no matter what biaxial in-plane loading it is subject to. Similar feature is also evident from the necking limit diagram of elastomer-supported metal layers of different hardening indices (i.e., $N = 0.1$ and 0.2 in Fig. 4c and e, respectively). The above results can be explained as follows. The elastomer substrate that follows a neo-Hookean constitutive law does not suffer from necking instability. So if the elastomer substrate is sufficiently stiff and/or thick, its mechanical constraint to the metal layer can be strong enough to override the necking instability of the metal layer. This agrees with previous bifurcation analysis and finite element simulations of an elastomer-supported metal film under plane-strain tension, in which the neo-Hookean elastomer is shown to harden substantially so that it can carry the metal film to deform uniformly to a large strain.

To further elaborate the above feature, Fig. 5 plots the critical value of S above which an elastomer-supported metal layer becomes immune from long wavelength necking instability as a function of biaxial loading ratio, for three hardening indices of the metal layer $N = 0.02, 0.1$ and 0.2 , respectively. In other words, each curve in Fig. 5 delineates a boundary, below (or above) which necking instability could (or not) occur, for a given value of N . Clearly there exists a maximum value of S , above which the metal layer is immune from necking instability under any arbitrary biaxial in-plane loadings. Such a maximum value of S decreases as N increases, i.e., $S = 0.93, 0.71$ and 0.54 , for $N = 0.02, 0.1$ and 0.2 , respectively. Fig. 5 can offer guidelines for structure design and material selection of elastomer-supported metal layers that are resistant to necking instability.

Similar to that in a plastic-supported metal layer, in positive loading ratio regime, the necking band in an elastomer-supported metal layer, if occurs, is always along the direction perpendicular to that of the greater tensile strain (i.e., $\theta = 0$), while in negative loading ratio regime, the necking band could appear in a slanted direction. Fig. 4b, d and f plot the necking band inclination angle θ as a function of a negative loading ratio ρ , for various values of S and N , corresponding to Fig. 4a, c and e, respectively. The dependence of θ on ρ is similar to that in a plastic-supported metal layer (Fig. 3b and d). It is worth to note here that, for a large value of S (e.g., $S = 0.9, 0.6$ and 0.5 for $N = 0.02, 0.1$ and 0.2 , respectively), it is possible that the necking band in an elastomer-supported metal layer is always perpendicular to that of the greater tensile strain ($\theta = 0$).

Fig. 6 plots necking limit strain of an elastomer-supported metal layer as a function of S under three representative loading ratios, i.e., uniaxial tension, plane-strain tension, and equi-biaxial tension, for $N = 0.02, 0.1$ and 0.2 , respectively. Necking limit strain increases as S increases, indicating a thicker and stiffer elastomer substrate leads to more necking retardation. In

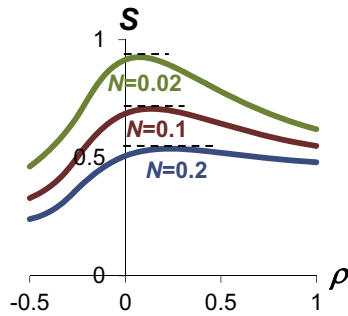


Fig. 5. Critical value of S above which an elastomer-supported metal layer becomes immune from necking instability as a function of biaxial loading ratio, for three hardening indices of the metal layer $N = 0.02, 0.1$ and 0.2 , respectively.

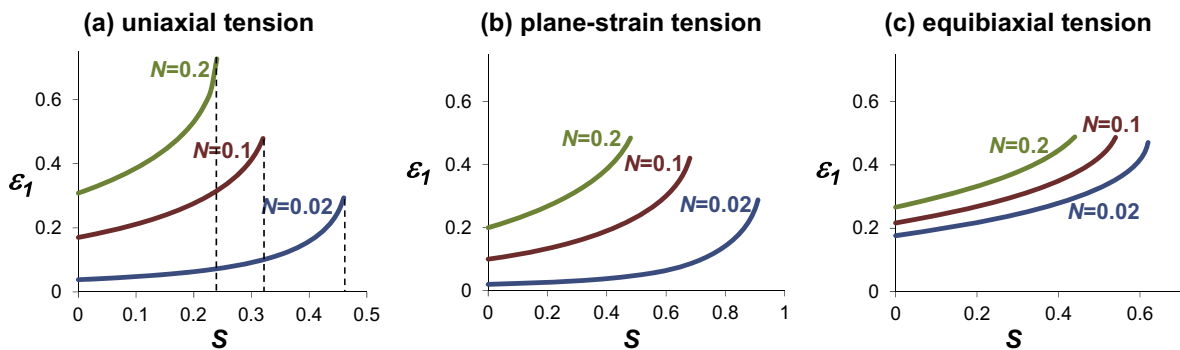


Fig. 6. Necking limit strain of an elastomer-supported metal layer as a function of S under (a) uniaxial tension, (b) plane-strain tension, and (c) equibiaxial tension, for $N = 0.02, 0.1$ and 0.2 , respectively. Note that $S = 0$ corresponds to the limiting case of a freestanding metal layer.

each loading ratio in Fig. 6, the higher hardening index, the larger necking limit strain, for a given value of S . For a given combination of hardening index and S , the necking limit strain in plane-strain tension is lower than those in uniaxial tension and equi-biaxial tension, a trend similar to that in a plastic-supported metal layer. All curves in Fig. 6 end at a critical value of S (e.g., as indicated by the dashed lines in Fig. 6a), above which the elastomer-supported metal layer becomes immune from necking instability.

To further facilitate the comparison with the commonly performed uniaxial tension experiments of elastomer-supported metal layers, Fig. 7 plots the necking band inclination angle θ under uniaxial tension as a function of S , for $N = 0.02, 0.1$ and 0.2 . Results show that, under uniaxial tension, a higher hardening index of the metal layer and a stiffer (and/or thicker) elastomer substrate result in a more slanted necking band. The predicted inclination angle of the necking band ranges from 35° to 45° , which agrees with existing experimental observations (Xiang et al., 2005b; Lu et al., 2010; Macionczyk and Bruckner, 1999; Gruber et al., 2004).

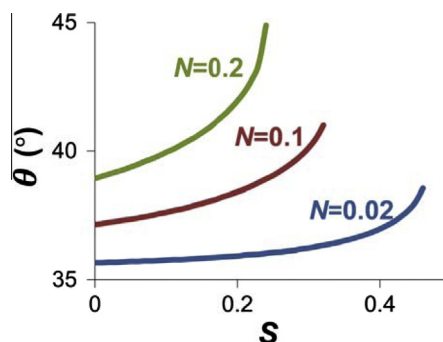


Fig. 7. Necking band inclination angle θ of an elastomer-supported metal layer under uniaxial tension as a function of S , for $N = 0.02, 0.1$ and 0.2 .

3.4. Enhanced energy absorption and dissipation in elastomer-supported metal layers under biaxial in-plane loading

The necking retardation in elastomer-supported metal layers further implies that a metal layer well bonded to an elastomer substrate could absorb or dissipate more energy prior to onset of necking than a single metal layer. Such a feature is of practical significance in engineering design of armor, in which enhanced energy absorption or dissipation is the key. One meaningful assessment of energy-absorption performance is to compare an elastomer-supported metal layer with a single all-metal layer with the same mass. Xue and Hutchinson (2007) conducted such a comparison and showed that, if the elastomer substrate is stiff enough, an elastomer-supported metal layer can absorb more energy prior to necking than an all-metal layer of same mass under plane-strain tension and equibiaxial tension. In this section, we compare the energy-absorption performance of an elastomer-supported metal layer with a single all-metal layer with the same mass over the full range of biaxial loading ratio in a similar procedure, and further consider the effective energy dissipation of the metal/elastomer bilayer if elastic recovery of the elastomer substrate occurs.

Let ρ^m and ρ^e be the densities of the metal and elastomer, respectively, and h_s be the initial thickness of the single all-metal layer. The mass per initial in-plane area, m_0 , is defined by

$$m_0 = \rho^m h + \rho^e H = \rho^m h_s. \tag{53}$$

The energy density absorbed by the metal layer, W^m , or elastomer substrate, W^e , prior to necking is

$$W^m = \frac{1}{1+N} K \varepsilon_{eff}^{N-1} = \frac{1}{1+N} K \left(2 \sqrt{\frac{1+\rho+\rho^2}{3}} \varepsilon_1 \right)^{N-1}, \tag{54}$$

$$W^e = \frac{E}{6} (\lambda_1^2 + \lambda_2^2 + \lambda_3^2 - 3) = \frac{E}{6} (e^{2\varepsilon_1} + \varepsilon^{2\rho\varepsilon_1} + e^{-2(1+\rho)\varepsilon_1} - 3), \tag{55}$$

where the necking strain ε_1 is evaluated by (49). The energies per initial area absorbed by the metal/elastomer bilayer or the all-metal single-layer prior to necking are

$$U_{single\ layer} = h_s W^m, \tag{56}$$

$$U_{bilayer} = h W^m + H W^e, \tag{57}$$

which are evaluated at their respective necking limit strains. Accounting for the equal-mass condition (53), the ratio of total absorbed energy in the metal-elastomer bilayer to that in the all-metal single-layer is given by

$$\left(\frac{U_{bilayer}}{U_{single\ layer}} \right)_{absorbed} = \frac{1}{1 + \frac{\rho^e h}{\rho^m H}} \left(\frac{(W^m)_{bilayer}}{(W^m)_{single\ layer}} + \frac{h}{H} \frac{W^e}{(W^m)_{single\ layer}} \right). \tag{58}$$

Prior to necking, the absorbed energy in a bilayer includes the plastic dissipation of the metal layer and the recoverable elastic energy in the elastomer substrate. In the limiting case of full release of the elastic energy (e.g., peeling off of the elastomer substrate after severe deformation), the ratio of effective dissipated energies in these two structures can be given by dropping the elastic energy term W^e in (58), which becomes

$$\left(\frac{U_{bilayer}}{U_{single\ layer}} \right)_{dissipated} = \frac{1}{1 + \frac{\rho^e H}{\rho^m h}} \left(\frac{(W^m)_{bilayer}}{(W^m)_{single\ layer}} \right). \tag{59}$$

The two ratios defined in (58) and (59) are functions of five dimensionless parameters: ρ^e/ρ^m , H/h , E/K , ρ and N . Here ρ^e/ρ^m is taken to be 0.1, representative of general elastomers and metals (e.g., polyurethane-supported steel plates). Fig. 8 plots these

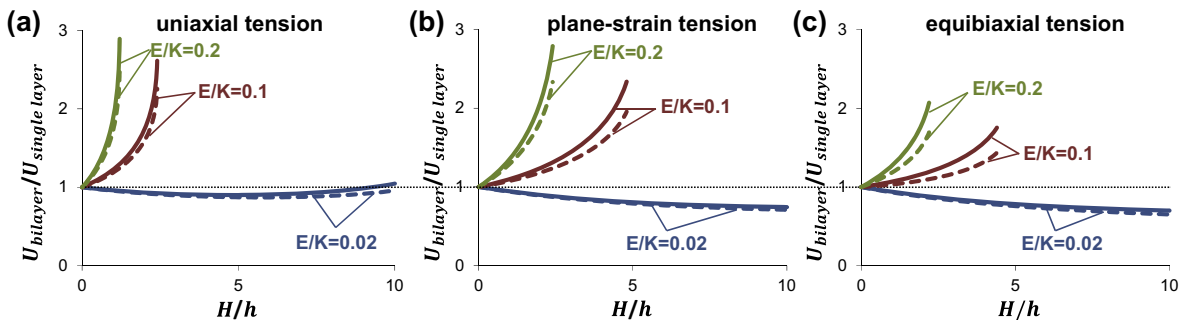


Fig. 8. Ratio of the energy absorbed (solid lines) or dissipated (dashed lines) at the onset of necking for a metal-elastomer bilayer to that of an all-metal single layer with the same mass as a function of the thickness ratio H/h , for $E/K = 0.02, 0.1$ and 0.2 . Here $N = 0.2$. (a) uniaxial tension, (b) plane-strain tension, and (c) equibiaxial tension. The horizontal dashed line represents energy ratio of 1.

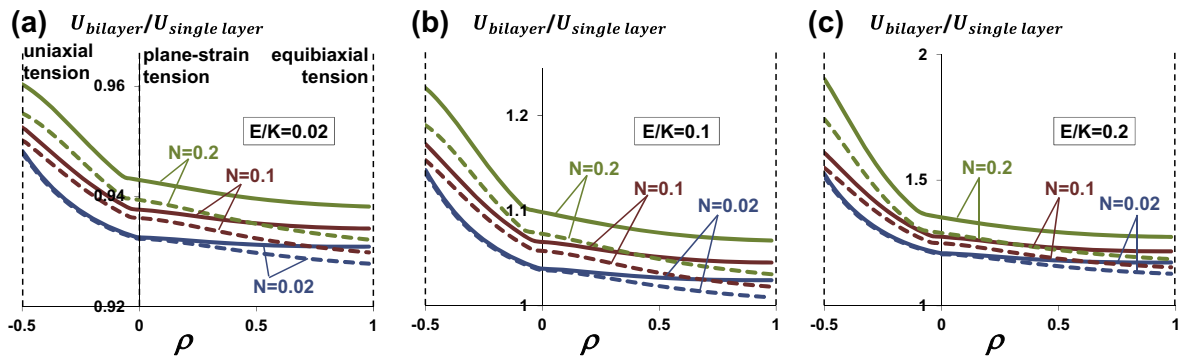


Fig. 9. Ratio of the energy absorbed (solid lines) or dissipated (dashed lines) at the onset of necking for a metal-elastomer bilayer plate to that of an all-metal single layer with the same mass as a function of the loading ratio ρ , for $N = 0.02, 0.1$ and 0.2 . Here $H/h = 1$. (a) $E/K = 0.02$, (b) $E/K = 0.1$, and (c) $E/K = 0.2$.

two ratios as functions of initial thickness ratio H/h for various values of E/K , under three representative types of in-plane loading, i.e., uniaxial tension (Fig. 8a), plane-strain tension (Fig. 8b) and equibiaxial tension (Fig. 8c), respectively. These curves demonstrate the effect of an elastomer substrate on enhancing energy absorption and dissipation in a metal layer. For all three types of in-plane loading, if E/K is sufficiently large (e.g., >0.1), both ratios are greater than 1 and increase as H/h increases. In other words, by replacing metal with elastomer without increasing overall mass, the elastomer-supported metal layer can absorb and dissipate more energy than the all-metal single layer. The thicker the elastomer substrate, the more enhanced energy absorption and dissipation performance. If H/h (and therefore S) is sufficiently large, the elastomer-supported metal layer becomes immune from necking instability (e.g., Fig. 6), the two energy ratios tends to infinity, as indicated by the termination of the curves in Fig. 8. If E/K is small (e.g., $=0.02$), both ratios are less than 1; so substituting a compliant elastomer for metal could jeopardize the energy absorption performance of the metal layer. Also evident in Fig. 8 is that the difference between the absorbed energy and the dissipated energy (or the elastic energy in the elastomer) is negligible for all cases. This result is of practical significance in the sense that, a proper elastomer substrate can effectively retard the necking occurrence in a metal layer, and more importantly, the resulting enhancement in the energy-absorption performance of the metal layer is robust even if the elastomer substrate fractures after the onset of metal necking.

To illustrate the effects of N and E/K on energy absorption and dissipation ratios under full range of biaxial in-plane loading, we consider a bilayer with equal metal and elastomer thicknesses ($H/h = 1$, e.g., by coating a metal layer with another layer of elastomer). Fig. 9 plots the energy absorption and dissipation ratios as functions of ρ , for $N = 0.02, 0.1$ and 0.2 and $E/K = 0.02, 0.1$ and 0.2 , respectively. If E/K is sufficiently large (e.g., >0.1 , Fig. 9b and c), both energy absorption and dissipation ratios are greater than 1 under any biaxial in-plane loading, while a too compliant elastomer substrate (e.g., $E/K = 0.02$, Fig. 9a) reduces the energy absorption performance of the metal layer. Both energy absorption and dissipation ratios increase as hardening index N increases and loading ratio ρ decreases. Specifically, an elastomer-supported metal layer can absorb and dissipate the most energy under uniaxial tension and the least under equibiaxial tension.

4. Conclusions and remarks

We perform bifurcation analysis for the onset of necking instability of substrate-supported metal layers under biaxial in-plane loading over the range of loading ratio from 1 (equibiaxial), to 0 (plane-strain), and to $-1/2$ (uniaxial). Key findings are summarized below:

- The necking limit strain of a metal layer supported by a plastic or an elastomer substrate is higher than that of the counterpart freestanding metal layer, for any biaxial in-plane loading explored. The retarded necking in substrate-supported metal layers essentially results from the mechanical constraint of the substrate to the metal layer deformation.
- The necking limit of a plastic/metal bilayer depends on four parameters: the loading ratio $\rho (= \varepsilon_2/\varepsilon_1)$, the hardening indices of the metal N_m and of the substrate N_s , and a dimensionless group $S = (K_s H)/(K_m h)$. The larger N_s and S , the more significant necking retardation. The necking limit strain of the freestanding plastic substrate sets the upper limit of retarded necking strain of the plastic/metal bilayer.
- The necking limit of an elastomer/metal bilayer depends on three parameters: the loading ratio ρ , the hardening index of the metal N , and a dimensionless group $S = (EH)/(K_m h)$. Supported by a sufficiently stiff and thick elastomer substrate, a metal layer can become immune from necking instability under any biaxial in-plane loading.
- In positive loading ratio regime, the necking band in substrate-supported metal layers, if occurs, is always along the direction perpendicular to that of the greater tensile strain. In negative loading ratio regime, the necking band could appear in a slanted direction. The maximum inclination angle of the necking band occurs under uniaxial tension. The predicted inclination angle from bifurcation analysis agrees well with the orientation of the necking bands in uniaxial tension experiments of substrate-supported metal layers.

- By replacing metal with a sufficiently stiff elastomer without increasing overall mass, an elastomer-supported metal layer can absorb and dissipate more energy than the all-metal single layer. The enhanced energy absorption and dissipation is robust even if the elastomer fractures after metal necking.

We conclude by a few remarks on the above findings. The necking limit analysis in the present study is based on a bifurcation analysis at the long-wavelength limit. In other words, a single diffusive neck is assumed to occur in an infinitely large substrate-supported metal layer. Previous bifurcation analysis of plastic-supported metal films (Li et al., 2005a) under plane-strain tension reveals that the lowest bifurcation strain corresponds to surface instability (short-wavelength), instead of necking instability (long-wavelength). While for an elastomer-supported metal film under plane-strain tension, the lowest bifurcation strain could correspond to non-uniform deformation at an intermediate wavelength (Li et al., 2004; Xue and Hutchinson, 2008). In other words, multiple necks could appear upon the onset of failure. In this sense, an all-wavelength bifurcation analysis is needed to fully understand the deformation instability of substrate-supported metal layers under biaxial in-plane loading.

The substrate-metal interface is assumed to be well bonded in the present analysis. In reality, interfacial delamination may occur in the substrate-metal bilayer under severe in-plane loading. Without the mechanical constraint from the substrate, the debonded portion of the metal layer is subject to necking instability more easily. Necking development and interfacial delamination can facilitate each other and co-evolve (Li et al., 2005a; Li and Suo, 2007; Lu et al., 2007). It is shown that the interfacial compliance plays a role in the deformation bifurcation of a substrate-supported layer (Bigoni et al., 1997). These aforementioned effects are desirable but beyond the scope of this paper, and we will report further studies in these regards elsewhere.

The present study considers substrate-supported metal layer subject to quasi-static biaxial in-plane loading. Under dynamic loading, the stretchability of an elastomer-supported metal ring can be significantly enhanced by forming multiple necks, a consequence of inertial stabilization (Guduru and Freund, 2002; Shenoy and Freund, 1999; Sorensen and Freund, 2000; Xue and Hutchinson, 2008). Fundamentally, the effects of geometrical constraint from the substrate and inertial stabilization under dynamic loading are not mutually exclusive to each other. Therefore, it is reasonable to expect that the necking retardation and associated enhancement in energy absorption and dissipation be still on effect for a substrate-supported metal layer under dynamic biaxial in-plane loading. Further work is needed to clarify the interplay of these two mechanisms on the necking instability of substrate-supported metal layers under dynamic loading. We also call for further experimental studies to demonstrate the research findings from the present theoretical study.

Conflicts of interests

The author declare that there is no conflicts of interest.

Acknowledgements

This research is supported by the U.S. National Science Foundation (Grants Nos. 0856540, 0928278 and 1069076). The authors are indebted to Prof. J.W. Hutchinson and Prof. J.R. Rice for their invaluable discussions and incisive comments on this work.

References

- Alaca, B.E., Saif, M.T.A., Sehitoglu, H., 2002. On the interface debond at the edge of a thin film on a thick substrate. *Acta Mater.* 50, 1197–1209.
- Amini, M., Nemat-Nasser, S., 2010. Micromechanisms of ductile fracturing of DH-36 steel plates under impulsive loads and influence of polyurea reinforcing. *Int. J. Fract.* 162, 205–217.
- Amini, M.R., Isaacs, J., Nemat-Nasser, S., 2010. Investigation of effect of polyurea on response of steel plates to impulsive loads in direct pressure-pulse experiments. *Mech. Mater.* 42, 628–639.
- Barlat, F., 1987. Crystallographic texture, anisotropic yield surfaces and forming limits of sheet metals. *Mater. Sci. Eng.* 91, 55–72.
- Benallal, A., Tvergaard, V., 1995. Nonlocal continuum effects on bifurcation in the plane-strain tension-compression test. *J. Mech. Phys. Solids* 43, 741–770.
- Bigoni, D., Ortiz, M., Needleman, A., 1997. Effect of interfacial compliance on bifurcation of a layer bonded to a substrate. *Int. J. Solids Struct.* 34, 4305–4326.
- Biot, M.A., 1965. *Mechanics of Incremental Deformations*. John Wiley and Sons, Inc.
- Brunet, M., Morestin, F., 2001. Experimental and analytical necking studies of anisotropic sheet metals. *J. Mater. Process. Technol.* 112, 214–226.
- Chiu, S.L., Leu, J., Ho, P.S., 1994. Fracture of metal-polymer line structures. I. Semiflexible polyimide. *J. Appl. Phys.* 76, 5136–5142.
- Consideré, A., 1885. *Memoire sur l'emploi du fer et de l'acier dans les constructions*. *Ann. Ponts Chaussées* 9, 574–775.
- Cordill, M.J., Taylor, A., Schalko, J., Dehm, G., 2010. Fracture and delamination of chromium thin films on polymer substrates. *Metall. Mater. Trans. A* 41A, 870–875.
- Cotton, D.P.J., Graz, I.M., Lacour, S.P., 2009. A multifunctional capacitive sensor for stretchable electronic skins. *IEEE Sens. J.* 9, 2008–2009.
- Espinosa, H.D., Prorok, B.C., Fischer, M., 2003. A methodology for determining mechanical properties of freestanding thin films and MEMS materials. *J. Mech. Phys. Solids* 51, 47–67.
- Franz, G., Abed-Meraim, F., Berveiller, M., 2013. Strain localization analysis for single crystals and polycrystals: towards microstructure–ductility linkage. *Int. J. Plast.*, doi: <http://dx.doi.org/10.1016/j.ijplas.2013.1002.1001>.
- Franz, G., Abed-Meraim, F., Lorrain, J., Ben Zineb, T., Lemoine, X., Berveiller, M., 2009. Ellipticity loss analysis for tangent moduli deduced from a large strain elastic-plastic self-consistent model. *Int. J. Plast.* 25, 205–238.
- Graudejus, O., Jia, Z., Li, T., Wagner, S., 2012. Size-dependent rupture strain of elastically stretchable metal conductors. *Scr. Mater.* 66, 919–922.
- Gruber, P., Bohm, J., Wanner, A., Sauter, L., Spolenak, R., Arzt, E., 2004. Size effect on crack formation in Cu/Ta and Ta/Cu/Ta thin film systems. *Materials Research Society Symposium Proceedings*, vol. 821, p. P2.7.1.

- Guduru, P.R., Freund, L.B., 2002. The dynamics of multiple neck formation and fragmentation in high rate extension of ductile materials. *Int. J. Solids Struct.* 39, 5615–5632.
- Haddag, B., Abed-Meraim, F., Balan, T., 2009. Strain localization analysis using a large deformation anisotropic elastic-plastic model coupled with damage. *Int. J. Plast.* 25, 1970–1996.
- Hashiguchi, K., Protasov, A., 2004. Localized necking analysis by the subloading surface model with tangential-strain rate and anisotropy. *Int. J. Plast.* 20, 1909–1930.
- Hill, R., 1970. Constitutive inequalities for isotropic elastic solids under finite strain. *Proc. R. Soc. London Ser. A* 314, 457–472.
- Hill, R., Hutchinson, J.W., 1975. Bifurcation phenomena in plane tension test. *J. Mech. Phys. Solids* 23, 239–264.
- Hommel, M., Kraft, O., 2001. Deformation behavior of thin copper films on deformable substrates. *Acta Materialia* 49, 3935–3947.
- Huang, H.B., Spaepen, F., 2000. Tensile testing of free-standing Cu, Ag and Al thin films and Ag/Cu multilayers. *Acta Mater.* 48, 3261–3269.
- Hutchinson, J.W., Neale, K.W., 1978. Sheet necking-II. Time-independent behavior. *Mechanics of Sheet Metal Forming*. Plenum Publishing Corporation, pp. 127–153.
- Hutchinson, J.W., Neale, K.W., Needleman, A., 1978. Sheet necking-I. Validity of plane stress assumptions of the long-wavelength approximation. *Mechanics of Sheet Metal Forming*. Plenum Publishing Corporation, pp. 111–126.
- Keller, R.R., Phelps, J.M., Read, D.T., 1996. Tensile and fracture behavior of free-standing copper films. *Materials Science and Engineering a-Structural Materials Properties Microstructure and Processing* 214, 42–52.
- Kuroda, M., Tvergaard, V., 2000. Forming limit diagrams for anisotropic metal sheets with different yield criteria. *Int. J. Solids Struct.* 37, 5037–5059.
- Lacour, S.P., Chan, D., Wagner, S., Li, T., Suo, Z., 2006. Mechanisms of reversible stretchability of thin metal films on elastomeric substrates. *Appl. Phys. Lett.* 88, 204103.
- Lacour, S.P., Jones, J., Wagner, S., Li, T., Suo, Z., 2005. Stretchable interconnects for elastic electronic surfaces. *Proc. IEEE* 93, 1459–1467.
- Li, T., Huang, Z., Suo, Z., Lacour, S., Wagner, S., 2004. Stretchability of thin metal films on elastomer substrates. *Appl. Phys. Lett.* 85, 3435–3437.
- Li, T., Huang, Z., Xi, Z., Lacour, S., Wagner, S., Suo, Z., 2005a. Delocalizing strain in a thin metal film on a polymer substrate. *Mech. Mater.* 37, 261–273.
- Li, T., Suo, Z., 2006. Deformability of thin metal films on elastomer substrates. *Int. J. Solids Struct.* 43, 2351–2363.
- Li, T., Suo, Z., 2007. Ductility of thin metal films on polymer substrates modulated by interfacial adhesion. *Int. J. Solids Struct.* 44, 1696–1705.
- Li, T., Suo, Z., Lacour, S., Wagner, S., 2005b. Compliant thin film patterns of stiff materials as platforms for stretchable electronics. *J. Mater. Res.* 20, 3274–3277.
- Lu, N.S., Suo, Z.G., Vlassak, J.J., 2010. The effect of film thickness on the failure strain of polymer-supported metal films. *Acta Mater.* 58, 1679–1687.
- Lu, N.S., Wang, X., Suo, Z.G., Vlassak, J., 2007. Metal films on polymer substrates stretched beyond 50%. *Appl. Phys. Lett.* 91, 221909.
- Macionczyk, F., Bruckner, W., 1999. Tensile testing of AlCu thin films on polyimide foils. *J. Appl. Phys.* 86, 4922–4929.
- Marciniak, Kuczynski, K., Pokora, T., 1973. Influence of plastic properties of a material on forming limit diagram for sheet-metal in tension. *Int. J. Mech. Sci.* 15, 789–800.
- Mercier, S., Granier, N., Molinari, A., Llorca, F., Buy, F., 2010. Multiple necking during the dynamic expansion of hemispherical metallic shells, from experiments to modelling. *J. Mech. Phys. Solids* 58, 955–982.
- Mercier, S., Molinari, A., 2003. Predictions of bifurcation and instabilities during dynamic extension. *Int. J. Solids Struct.* 40, 1995–2016.
- Morales, S.A., Albrecht, A.B., Zhang, H., Liechti, K.M., Ravi-Chandar, K., 2011. On the dynamics of localization and fragmentation: V. Response of polymer coated Al 6061-O tubes. *Int. J. Fract.* 172, 161–185.
- Needleman, A., Tvergaard, V., 1977. Necking of biaxially stretched elastic-plastic circular plates. *J. Mech. Phys. Solids* 25, 159–183.
- Neil, C., Agnew, S., 2009. Crystal plasticity-based forming limit prediction for non-cubic metals: application to Mg alloy AZ31B. *Int. J. Plast.* 25, 379–398.
- Nicola, L., Xiang, Y., Vlassak, J.J., Van der Giessen, E., Needleman, A., 2006. Plastic deformation of freestanding thin films: experiments and modeling. *J. Mech. Phys. Solids* 54, 2089–2110.
- Niu, R.M., Liu, G., Wang, C., Zhang, G., Ding, X.D., Sun, J., 2007. Thickness dependent critical strain in submicron Cu films adherent to polymer substrate. *Appl. Phys. Lett.* 90, 161907.
- Pashley, D., 1960. A study of the deformation and fracture of single-crystal gold films of high strength indise an electron microscope. *Proc. R. Soc. London Ser. A* 255, 218–231.
- Shenoy, V.B., Freund, L.B., 1999. Necking bifurcations during high strain rate extension. *J. Mech. Phys. Solids* 47, 2209–2233.
- Sorensen, N.J., Freund, L.B., 2000. Unstable neck formation in a ductile ring subjected to impulsive radial loading. *Int. J. Solids Struct.* 37, 2265–2283.
- Storen, S., Rice, J.R., 1975. Localized necking in thin sheets. *J. Mech. Phys. Solids* 23, 421–441.
- Stoughton, T.B., 2000. A general forming limit criterion for sheet metal forming. *Int. J. Mech. Sci.* 42, 1–27.
- Tvergaard, V., Needleman, A., Lo, K.K., 1981. Flow localization in the plane-strain tensile test. *J. Mech. Phys. Solids* 29, 115–142.
- Wagner, S., Lacour, S., Jones, J., Hsu, P., Sturm, J., Li, T., Suo, Z., 2004. Electronic skin: architecture and components. *Phys. E Low Dimens. Syst. Nanostruct.* 25, 326–334.
- Xiang, Y., Chen, X., Vlassak, J.J., 2005a. Plane-strain bulge test for thin films. *J. Mater. Res.* 20, 2360–2370.
- Xiang, Y., Li, T., Suo, Z., Vlassak, J., 2005b. High ductility of a metal film adherent on a polymer substrate. *Appl. Phys. Lett.* 87, 161910.
- Xu, W., Lu, T.J., Wang, F., 2010. Effects of interfacial properties on the ductility of polymer-supported metal films for flexible electronics. *Int. J. Solids Struct.* 47, 1830–1837.
- Xue, Z., Vaziri, A., Hutchinson, J.W., 2008. Material aspects of dynamic neck retardation. *J. Mech. Phys. Solids* 56, 93–113.
- Xue, Z.Y., Hutchinson, J.W., 2007. Neck retardation and enhanced energy absorption in metal-elastomer bilayers. *Mech. Mater.* 39, 473–487.
- Xue, Z.Y., Hutchinson, J.W., 2008. Neck development in metal/elastomer bilayers under dynamic stretchings. *Int. J. Solids Struct.* 45, 3769–3778.
- Yu, D.Y.W., Spaepen, F., 2004. The yield strength of thin copper films on Kapton. *J. Appl. Phys.* 95, 2991–2997.
- Zhang, H., Liechti, K.M., Ravi-Chandar, K., 2009. On the dynamics of localization and fragmentation-III. Effect of cladding with a polymer. *Int. J. Fract.* 155, 101–118.
- Zhang, H., Ravi-Chandar, K., 2006. On the dynamics of necking and fragmentation – I. Real-time and post-mortem observations in Al6061-O. *Int. J. Fract.* 142, 183–217.
- Zhang, L., Wang, J., 2012. Modeling the localized necking in anisotropic sheet metals. *Int. J. Plast.* 39, 103–118.
- Zhao, L., Sowerby, R., Sklad, M.P., 1996. A theoretical and experimental investigation of limit strains in sheet metal forming. *Int. J. Mech. Sci.* 38, 1307–1317.